纳秒激光辐照划痕表面熔石英的热应力模型

卢强[1]，许卫洪[2]，王绶玙[1]，孔艳[1]，刘诚[1,3*]
[1]江南大学理学院计算光学实验室，江苏 无锡 214122；
[2]无锡商业职业技术学院物联网与人工智能学院，江苏 无锡 214153；
[3]中国科学院上海光学精密机械研究所，上海 201800

摘要 为了研究激光辐照含有表面划痕的熔石英的热应力特性,基于电磁场、热传导及弹塑性力学理论,建立了适用于不同表面缺陷类型的纳秒脉冲激光辐照熔石英的热应力数值模型。利用该模型计算得到平滑表面和划痕表面熔石英在激光辐照后的温度场分布和应力场分布,并通过搭建的激光损伤测试及应力在线测量系统实验验证了所建模型。研究结果表明,熔石英的表面结构引起的光场调制会导致激光辐照后熔石英内部应力增强,并且应力大小与其表面结构尺寸密切相关。研究结果不仅有助于分析含有表面划痕的光学元件的激光损伤机理及残余应力,而且能够对激光加工的热应力调控提供理论依据。

关键词 激光技术；激光损伤；应力分布；表面划痕；光场调制
中图分类号 O343.6 **文献标志码** A **DOI：** 10.3788/CJL221146

1 引 言

随着激光技术的不断发展,激光器的输出功率和单脉冲能量越来越高,其被广泛应用于激光加工、激光医疗、光通信和惯性约束核聚变等领域[1-3]。在高能量密度条件下,光学元件的抗激光损伤性能是影响高功率激光系统进一步发展的一个主要因素。实际上当激光脉冲的能量密度远低于光学材料的理论损伤阈值时,材料表面往往也会发生损伤(即实际损伤阈值低于理论损伤阈值),导致光学元件的工作寿命缩短以及高功率激光系统的峰值输出功率大大降低[4-6]。光学元件在激光辐照后产生损伤,不仅会影响输出激光的光束质量,使得系统的光学性能下降[7-9],而且会进一步产生损伤增长并引起下游其他光学元件的损伤[10-13],严重限制了高功率激光的应用与发展。因此研究光学材料在高功率激光辐照下的损伤特性具有十分重要的意义。

激光损伤的机理是非常复杂的,涉及激光能量沉积、温度和应力变化以及材料相变等多个物理过程。在这些过程中,应力会导致光学元件出现凹坑和裂纹等多种类型的损伤,同时光学元件中的残余应力还加大了激光修复光学元件的难度,因此深入探究激光辐照光学材料的热应力特性是研究激光损伤的关键。Chambonneau等[14]研究了纳秒激光波长与熔石英损伤形貌的关系,发现355 nm纳秒激光引起的损伤主要是热应力损伤,而对于1064 nm激光,主要是等离子体的传播导致表面形成损伤环。Guignard等[15]利用干涉显微研究了熔石英和K9玻璃内部的应力分布。Gallais等[16]用光弹法研究了激光修复损伤点后其周围的残余应力分布。Zhu等[17]研究了激光辐照熔石英表面所产生的应力行为,发现损伤形貌与应力状态相关。Rehman等[18]研究了脉冲激光辐照熔石英过程中的微爆炸现象,认为高压和高温共同导致了材料的相变。吴朱洁等[19]通过构建二维热力学模型,对玻璃前后表面的损伤形貌进行了研究,分析了前后表面的损伤形式以及主要因素。然而,这些热应力特性的相关研究都是针对表面平滑的光学材料,其实验和仿真结果不适用于具有各种表面缺陷或周期性结构的光学元件[20-24]。

光学元件在制造和使用过程中产生的划痕、裂纹、污染物等机械或化学缺陷会造成表面形貌变化,导致其激光损伤阈值降低。Ye等[25]利用不同类型的抛光液制造了具有表面划痕的熔石英样品,研究了划痕对损伤阈值的影响并仿真计算了不同划痕引起的光场增强。Wang等[26]利用砂纸在熔石英表面制造了人工缺陷,比较了不同缺陷密度熔石英的激光损伤阈值,并采用时域有限差分法模拟了裂纹周围的电场分布。Lu等[11]通过有限元法计算了多脉冲激光加工过程中的温度累积、应力产生及形貌变化对激光打孔性能的影响。然而,这些关于激光辐照含有表面缺陷的熔石英的研

收稿日期： 2022-08-15；**修回日期：** 2022-09-26；**录用日期：** 2022-10-11；**网络首发日期：** 2022-10-21
基金项目： 国家自然科学基金(12004141)、江苏省自然科学基金(BK20200588)

通信作者： *chengliu@siom.ac.cn

究主要集中在缺陷引起的光场增强及其对损伤阈值、损伤形貌的影响，目前仍然没有一个相对全面的热力学模型和实验来阐述具有表面缺陷的熔石英在激光辐照下的热应力特性。

本文建立了适用于平滑表面和缺陷表面的熔石英与纳秒激光脉冲相互作用的热应力模型，利用所建模型研究了平滑表面熔石英和划痕表面熔石英在激光脉冲辐照后的温度场和应力场，利用所搭建的激光损伤测试以及应力在线测量系统对模型准确性进行了验证，并且对比分析了平滑表面和划痕表面熔石英在纳秒激光脉冲辐照下的应力行为。

2　模型建立

本文使用有限元法建立了纳秒脉冲激光与材料相互作用的热应力模型，如图 1 所示，基于电磁场、热传导及弹塑性力学理论，首先对激光加热过程中材料内部的温度演变进行计算，再利用温度场计算材料内部的应力分布。

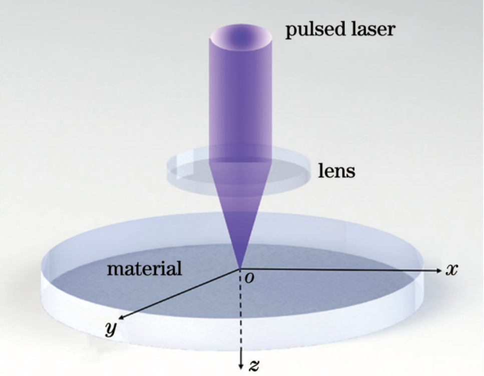

图 1　纳秒脉冲激光辐照光学材料的示意图

Fig. 1　Schematic of optical material irradiated by nanosecond pulse laser

在高功率激光辐照下，材料吸收激光能量，热量沉积在材料内部。在这个过程中，激光相当于一个具有一定时间和空间分布的热源。为了与本文实验中所使用的纳秒脉冲激光保持一致，设定入射的脉冲激光服从高斯分布，并正入射于样品的前表面。激光能量的空间分布$f(x,y)$和时间分布$g(t)$分别表示为

$$f(x,y)=\exp\left(-2\frac{x^2+y^2}{w_0^2}\right),\tag{1}$$

$$g(t)=\begin{cases}\exp\left[-\frac{2}{\tau^2}\left(t-\frac{\tau}{2}\right)\right], & 0<t\leqslant\tau\\ 0, & t>\tau\end{cases},\tag{2}$$

式中：w_0是$1/\mathrm{e}^2$处的激光光斑半径；τ是激光的脉宽。根据傅里叶热传导理论，激光辐照后材料内部的热量通过热传导扩散，其三维温度场$T(x,y,z,t)$的瞬态分布可以通过经典傅里叶热传导方程[27]来求解：

$$\nabla\left[k\nabla T(x,y,z,t)\right]=\rho c\frac{\partial T(x,y,z,t)}{\partial t}-Q(x,y,z,t),\tag{3}$$

式中：ρ、c、k分别是材料的密度、比热容、热导率；$Q(x,y,z,t)$是材料吸收激光脉冲能量后所产生的热源项。对于平滑表面的情况，激光能量在材料内部依旧服从高斯分布，另外根据朗伯-比尔定律，在材料内部激光能量发生指数衰减，因此平滑表面的热源项$Q(x,y,z,t)$一般可以表示为

$$Q(x,y,z,t)=\alpha P\frac{(1-R)}{\pi w_0^2}f(x,y)g(t)\exp(-\alpha z),\tag{4}$$

式中：α、P和R分别为材料对激光的吸收系数、激光功率以及材料的表面反射率。

而对于具有划痕、裂纹、凹坑等缺陷的表面而言，表面不平整导致激光在材料内部发生折射、衍射和干涉现象，从而极大地改变了激光在材料内部的能量分布，使其不再满足高斯分布，因此式(4)所描述的热源分布不再适用，此时必须考虑表面形貌对热源的影响。对于这种情况，需要对式(4)中的热源分布进行修正，含有表面缺陷的材料内部的热源为

$$Q(x,y,z,t)=\alpha P\frac{(1-R)}{\pi w_0^2}f(x,y)g(t)\times\\ \exp(-\alpha z)I_\mathrm{R}(x,y,z)。\tag{5}$$

为了考虑表面结构对材料内部光场的影响，在热源项中引入相对光强因子I_R，即含有表面缺陷的材料内部光强分布$\left|E_1\right|^2$与表面平滑的材料内部光强分布$\left|E_0\right|^2$的比值：

$$I_\mathrm{R}(x,y,z)=\frac{\left|E_1(x,y,z)\right|^2}{\left|E_0(x,y,z)\right|^2}。\tag{6}$$

另外，在温度场的求解过程中还考虑了热对流和热辐射对材料温度的影响[28]：

$$-k\left(\frac{\partial T}{\partial x}+\frac{\partial T}{\partial y}+\frac{\partial T}{\partial z}\right)=h(T-T_0)+\varepsilon B(T^4-T_0^4),\tag{7}$$

式中：h、ε和B分别表示自然对流系数、表面辐射系数和黑体辐射常数；T_0表示材料的初始温度。材料内部激光能量分布不均匀，使得激光辐照后材料的温度分布不均匀，从而导致热应力的产生。材料内部的热应力可以通过热弹性方程计算得到：

$$\sigma_x=\frac{E}{(1+\nu)(1-2\nu)}\left[\varepsilon_x+\nu(\varepsilon_y+\varepsilon_z-\varepsilon_x)\right]-\\ \frac{E\beta(T-T_0)}{1-2\nu},\tag{8}$$

$$\sigma_y=\frac{E}{(1+\nu)(1-2\nu)}\left[\varepsilon_y+\nu\left(\varepsilon_x+\varepsilon_z-\varepsilon_y\right)\right]-\frac{E\beta\left(T-T_0\right)}{1-2\nu},\tag{9}$$

$$\sigma_z=\frac{E}{(1+\nu)(1-2\nu)}\left[\varepsilon_z+\nu\left(\varepsilon_x+\varepsilon_y-\varepsilon_z\right)\right]-\frac{E\beta\left(T-T_0\right)}{1-2\nu},\tag{10}$$

式中：σ_x、σ_y和σ_z分别为x、y、z方向的热应力分量；ε_x、ε_y、ε_z分别为x、y、z方向的应变分量；E、ν和β分别为材料的杨氏模量、泊松比和热膨胀系数。

3　结果与分析

采用所建模型模拟355 nm纳秒激光辐照熔石英材料的热应力特性，计算所需参数如表1[7,29]所示。

表1　熔石英的热力学参数

Table 1　Thermodynamic parameters of fused silica

Parameter	Value
Density /(kg·m^{-3})	2200
Specific heat /[J·(kg·K)$^{-1}$]	750
Thermal expansion coefficient /K^{-1}	5.1×10^{-7}
Thermal conductivity /(W·mK^{-1})	1.38
Young's modulus /GPa	72.6
Poisson's ratio	0.16
Absorption coefficient /m^{-1}	200
Melting point /K	1800
Evaporation point /K	2500
Initial temperature /K	300

在激光波长为355 nm、脉冲宽度为5 ns的激光辐照下，单脉冲激光辐照平滑表面熔石英后的模拟结果如图2所示，其中图2(a)展示了平滑表面熔石英的示意图。在能量密度为11.1 J/cm^{2}的单脉冲辐照下，脉冲恰好结束即5 ns时熔石英内部的温度场分布如图2(b)所示，由于熔石英对激光能量的吸收，温度从初始温度300 K升高到最高温度1821 K，此时最高温度处于光斑中心，高于熔石英玻璃的熔化温度，发生熔融损伤。由于熔石英内部存在明显的温差，因此不可避免地会产生热应力，图2(c)显示了熔石英内部的应力分布。对于平滑表面的熔石英，激光在熔石英内部的能量分布未发生改变(即$I_R=1$)，因此温度分布、应力分布与熔石英内部激光能量的高斯分布是一致的。

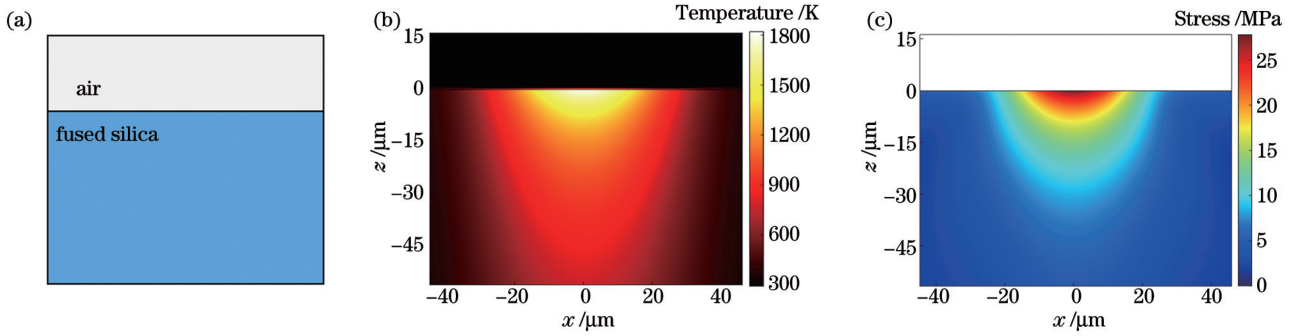

图2　能量密度为11.1 J/cm^{2}的单脉冲辐照平滑表面熔石英的模拟结果。(a)平滑表面熔石英的示意图；(b)温度分布；(c)应力分布

Fig. 2　Simulation results for fused silica with smooth surface irradiated by single pulse with energy density of 11.1 J/cm^2. (a) Diagram of fused silica with smooth surface; (b) temperature distribution; (c) stress distribution

脉冲激光辐照划痕表面熔石英的仿真结果如图3所示。图3(a)是表面划痕的示意图，划痕宽度为w，深度为d。图3(b)展示了能量密度为5.4 J/cm^{2}时激光辐照划痕表面(w=2 μm，d=1 μm)熔石英产生的相对光强因子分布，此时激光辐照表面划痕发生衍射效应，同时经过划痕侧壁的折射光和熔石英表面的透射光干涉，使得表面划痕对入射激光产生明显的调制作用，导致熔石英局部区域的激光能量增强。在能量密度为5.4 J/cm^{2}的单脉冲激光辐照下，划痕表面熔石英的温度场分布如图3(c)所示。划痕的调制作用使激光的能量在熔石英局部出现了增强和减弱，致使不同区域吸收的激光能量不同，导致在熔石英内部出现了温度条纹。图3(d)为激光辐照划痕表面熔石英所产生的应力场分布，温度条纹的出现导致热膨胀极度不均匀，最终在划痕表面熔石英内部形成热应力条纹。由于表面划痕对光场的调制，与图2中平滑表面熔石英在11.1 J/cm^{2}激光能量密度下发生熔融相比，划痕表面熔石英在5.4 J/cm^{2}能量密度下就达到了熔点，并且其内部的温度场、热应力场都出现了条纹现象。

为了验证上述数值模型的准确性，搭建了激光损伤测试以及应力在线测量系统，实验装置图如图4所示。整个光路系统可以分为两部分，一部分是激光损伤光路，另一部分是损伤形貌探测和应力测量光路。激光损伤光路主要由脉冲激光器、半波片、格兰棱镜、聚焦透镜(lens 1)和熔石英样品组成。其中，脉冲激光器是波长为355 nm、脉冲宽度为5 ns的Nd:YAG激光器；通过调节半波片和格兰棱镜之间的相对角度来控制激光输出功率；透镜lens 1将激光聚焦到熔石英样

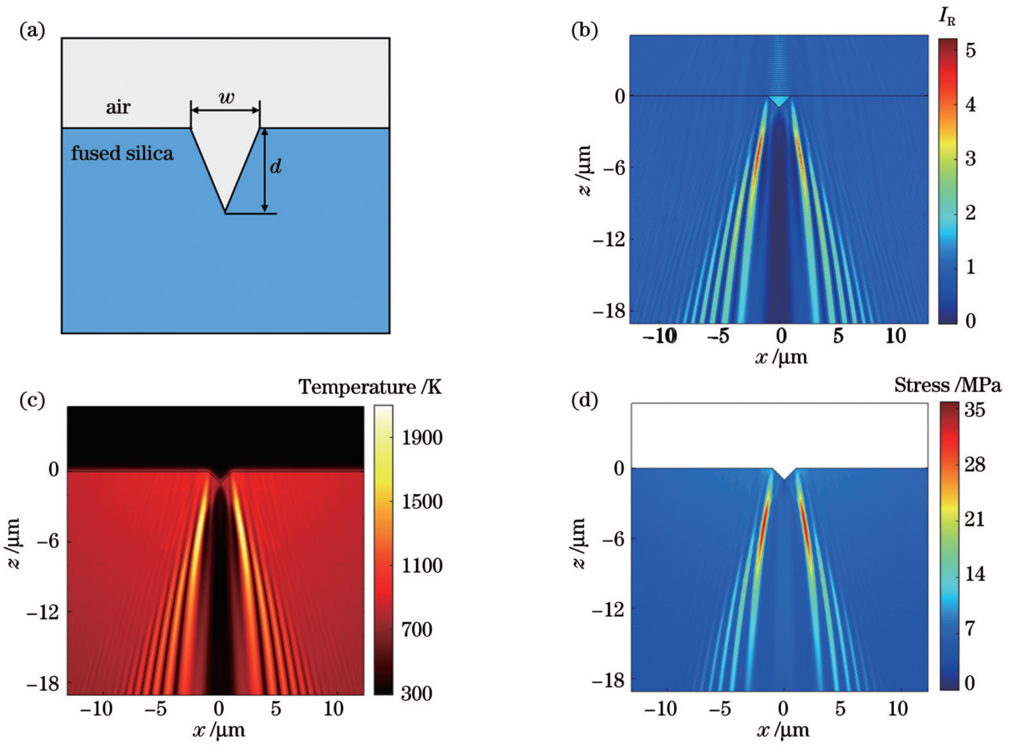

图 3　能量密度为 5.4 J/cm^{2}的单脉冲辐照划痕表面熔石英的仿真结果。(a)表面划痕示意图；(b)表面划痕引起的相对光强因子分布；(c)温度分布；(d)应力分布。

Fig. 3　Simulation results for fused silica with scratch surface irradiated by single pulse with energy density of 5.4 J/cm^2. (a) Diagram of surface scratch; (b) distribution of relative light intensity factor caused by surface scratch; (c) temperature distribution; (d) stress distribution

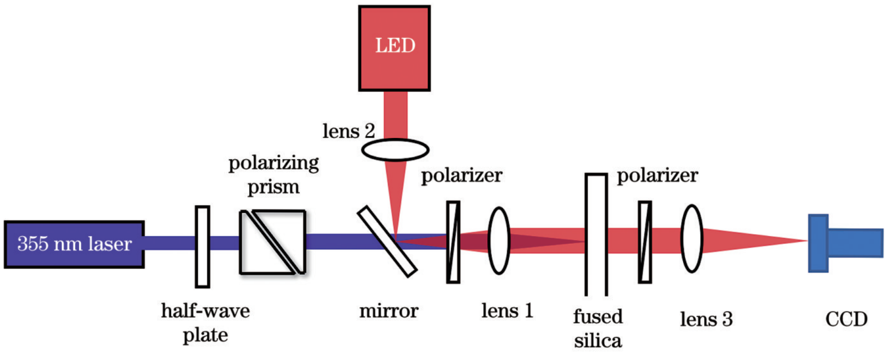

图 4　激光损伤测试以及应力在线测量系统的实验光路

Fig. 4　Experimental optical path of laser damage test and stress on-line measurement system

品的表面，光斑呈近高斯分布，光斑半径为 80 μm。熔石英样品的尺寸为 20 mm×20 mm×2 mm，表面粗糙度大约为 40 nm。在实验前使用去离子水对熔石英样品进行超声波清洗，然后再用乙醇进行擦拭。损伤形貌探测和应力测量光路主要由波长为 632.8 nm 的发光二极管（LED）光源、三个透镜（lens 1、lens 2 和 lens 3）、两个正交的偏振片、熔石英样品以及电荷耦合器件（CCD）相机组成。其中，透镜 lens 1 和 lens 2 在该光路中起准直作用，lens 3 是成像透镜；熔石英样品放置在两个正交的偏振片之间，通过光弹法对损伤点附近的应力进行测量；CCD 相机用来记录损伤形貌和应力相关分布图像。

通过搭建的激光损伤测试以及应力在线测量系统，首先对脉冲激光辐照平滑表面熔石英的结果进行验证，仿真和实验结果如图 5 所示。图 5(a1)～(a4)是能量密度为 662.1 J/cm^{2}的单脉冲激光辐照平滑表面的实验结果，其中图 5(a1)是熔石英样品表面产生的损伤形貌，图 5(a2)是两个偏振片正交时 CCD 相机记录的应力相关分布图像，图 5(a3)是两个偏振片都顺时针旋转 45°时得到的应力相关分布。通过获取的两个应力相关分布消除应力计算过程中产生的等倾线干扰，最终利用平面偏振光法[30-31]得到损伤点周围的应力分布，如图 5(a4)所示。值得注意的是，此时测得的是熔石英的二维应力分布，即应力在光轴（z 轴）方向

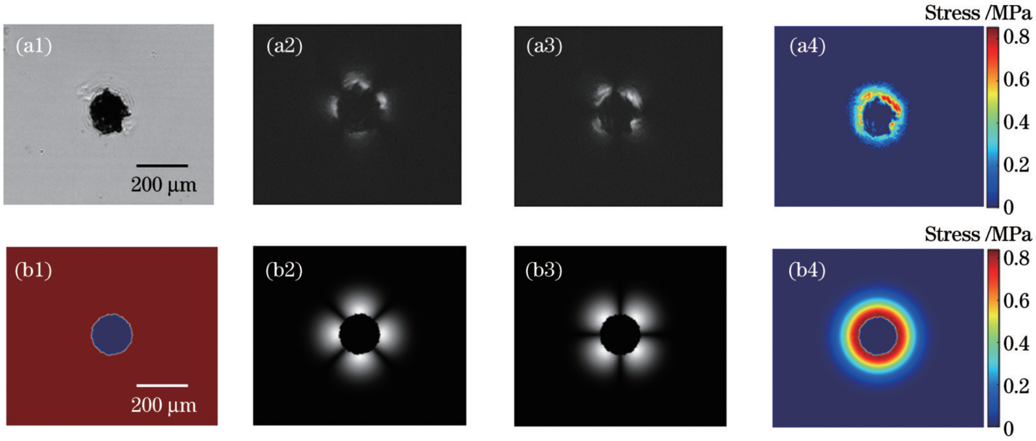

图 5　激光辐照平滑表面熔石英的实验和仿真结果。激光能量密度为 662.1 J/cm^{2}时损伤形貌的(a1)实验结果和(b1)仿真结果；正交偏振片旋转前的(a2)实验结果和(b2)仿真结果；正交偏振片同时旋转 45°时的(a3)实验结果和(b3)仿真结果；应力分布的(a4)实验结果和(b4)仿真结果

Fig. 5　Experimental and simulation results for fused silica with smooth surface irradiated by laser. (a1) Experimental result and (b1) simulation result of damage morphology at laser energy density of 662.1 J/cm^2; (a2) experimental result and (b2) simulation result before rotation of orthogonal polarizers; (a3) experimental result and (b3) simulation result after rotating orthogonal polarizers simultaneously by 45°; (a4) experimental result and (b4) simulation result of stress distribution

的平均值。图 5(b1)～(b4)是能量密度为 662.1 J/cm^{2}的单脉冲激光辐照平滑表面的模拟结果，其中图 5(b1)是仿真得到的损伤形貌，图 5(b2)和图 5(b3)分别是正交偏振片相差 45°时的应力相关分布图像，图 5(b4)是应力分布的仿真结果。可以看出，损伤形貌和应力分布的仿真结果与实验结果基本相符。图 6 显示了激光能量密度分别为 445.6、509.3、572.9 J/cm^{2}时单脉冲辐照熔石英样品的损伤形貌以及应力分布。激光能量密度与损伤点周围最大应力的关系如图 7 所示，当激光能量密度分别为 445.6、509.3、572.9、662.1 J/cm^{2}时，实验测得的应力最大值分别为 0.56、0.66、0.78、0.85 MPa，模型计算得到的应力分别为 0.58、0.68、0.77、0.84 MPa。实验和仿真结果对比可以发现，随着激光能量密度的增加，平滑表面熔石英的应力明显增大，并且激光辐照平滑表面熔石英的模型计算结果与实验结果基本一致。

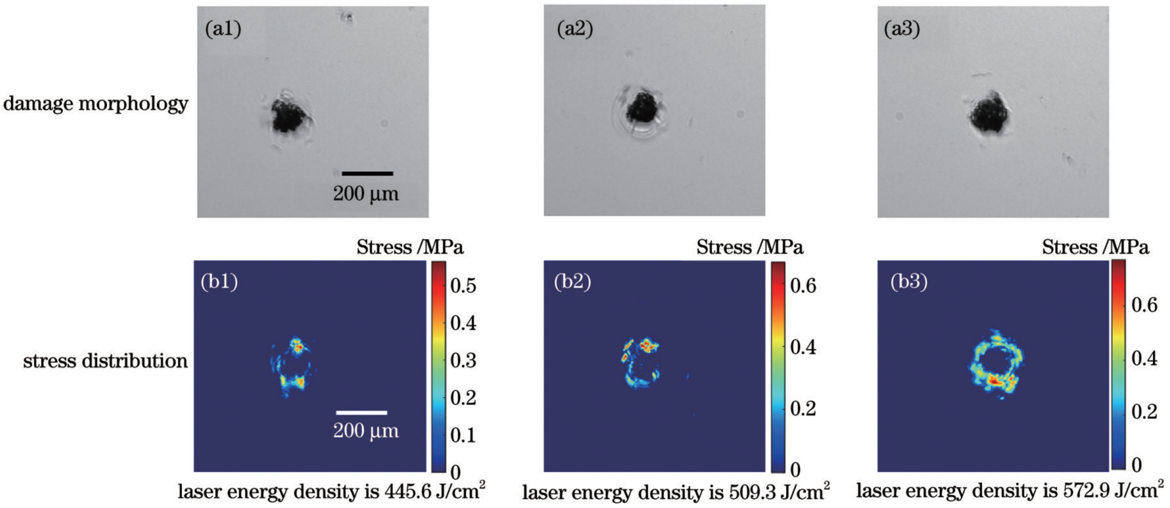

图 6　不同激光能量密度单脉冲辐照平滑表面熔石英的损伤形貌及应力分布

Fig. 6　Damage morphologies and stress distributions of fused silica with smooth surface irradiated by single pulses with different laser energy densities

使用金刚石玻璃刀在熔石英表面人工制造划痕，划痕的形貌如图 8 所示，划痕宽度为(8±2)μm，深度为(1.5±1.0)μm。在划痕制造过程中，熔石英内部会产生机械应力，并且划痕区域清洗后残余的碎颗粒会引起照明光散射，从而引起偏振转换，这两者都会干扰应力测量的实验结果。因此，在激光辐照前先用 CCD 相机记录熔石英样品的应力相关分布，从而在最后计算激光辐照所引起的应力时消除划痕本身带来的应力变化。纳秒激光脉冲辐照划痕表面熔石英的实验结果如图 9 所示，其中图 9(a1)～

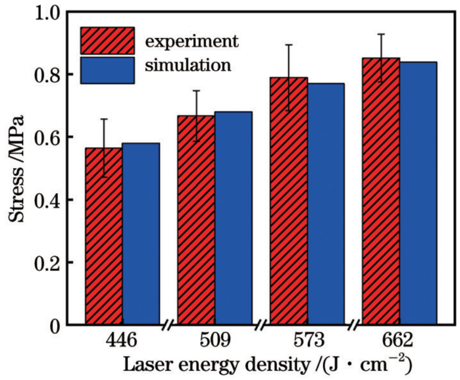

图 7 激光辐照平滑表面熔石英的最大应力随激光能量密度的变化

Fig. 7 Maximum stress of laser irradiated fused silica with smooth surface versus laser energy density

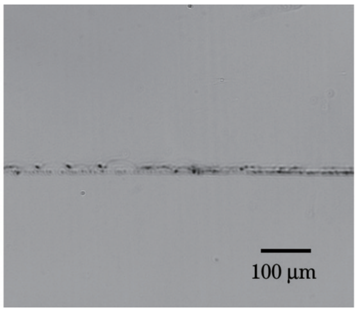

图 8 利用金刚石玻璃刀在熔石英表面制造的划痕形貌

Fig. 8 Scratch morphology on surface of fused silica made with diamond glass knife

（a3）显示了激光能量密度分别为 445.6、509.3、572.9 J/cm^{2}的单脉冲辐照划痕表面熔石英的损伤形貌，图 9（b1）～（b3）为对应激光能量密度下熔石英的应力分布。对于激光辐照划痕表面的情况，激光能量密度与损伤点周围最大应力的关系如图 10 所示，当激光能量密度分别为 445.6、509.3、572.9、662.1 J/cm^{2}时，实验测量的应力最大值（每个能量密度下重复 10 次实验，取 10 次应力最大值的平均值）分别为 1.11、1.16、1.25、1.27 MPa，模型计算得到的激光辐照划痕（w=8 μm，d=1.5 μm）的应力分别为 1.16、1.17、1.18、1.24 MPa。可以看出，激光辐照划痕表面熔石英所产生应力的模型计算结果与实验测量结果基本相符。

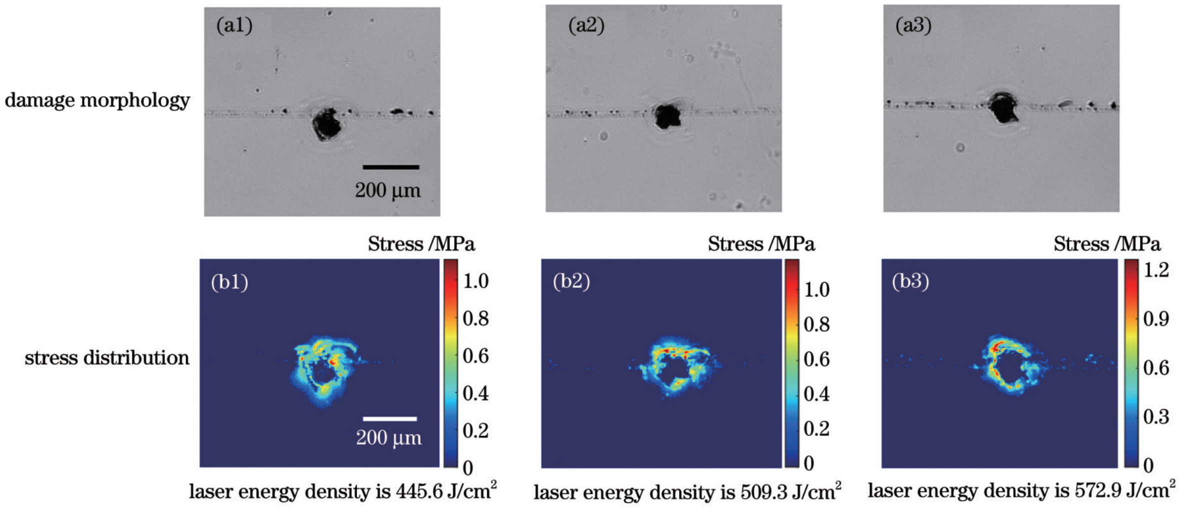

图 9 不同激光能量密度单脉冲辐照划痕表面熔石英的损伤形貌及应力分布

Fig. 9 Damage morphologies and stress distributions of fused silica with scratch surface irradiated by single pulses with different laser energy densities

对比激光辐照平滑表面熔石英（图 7）与激光辐照划痕表面熔石英（图 10）的实验结果，可以发现，当激光能量密度分别为 445.6、509.3、572.9、662.1 J/cm^{2}时，划痕表面熔石英产生的二维应力最大值分别为 1.11、1.16、1.25、1.27 MPa，平滑表面熔石英产生的二维应力最大值分别为 0.56、0.66、0.78、0.85 MPa，表明熔石英的表面划痕会导致激光辐照熔石英内部应力增强。而构建的热应力模型也能得到与实验一致的结果，模型计算得到的划痕表面熔石英产生的二维应力最大值分别为 1.16、1.17、1.18、1.24 MPa，平滑表面熔石英产生的二维应力最大值分别为 0.58、0.68、0.77、0.84 MPa。结合图 2 和图 3 中激光辐照平滑表面和划痕表面的仿真结果，发现表面划痕对光场的调制使得激光辐照后划痕表面熔石英内部应力增大。

实际出现在熔石英表面或内部的划痕尺寸与形貌各不相同，还会在一定范围内变化，并且在划痕的人为制造过程中也难以精确控制划痕的尺寸。对于激光辐照熔石英表面不同类型、不同尺寸的划痕所产生的热应力，实验研究方法存在工作量大且繁杂的缺点。而上述研究结果已经验证了我们所构建的热应力模型适用于激光辐照任意形状、任意尺寸表面划痕的仿真研究。图 11 给出了纳秒激光辐照划痕表面熔石英所产生的应力最大值与划痕宽度、深度的关系，激光能量密度为 5.4 J/cm^2，其中虚线是相同条件下

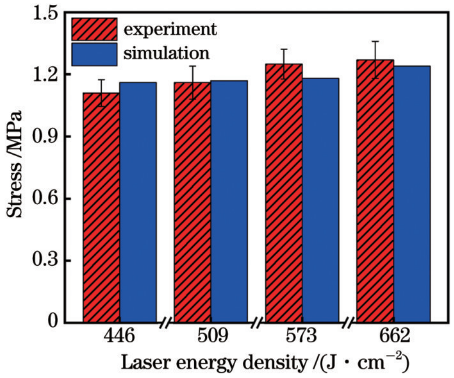

图10 激光辐照划痕表面熔石英的最大应力随激光能量密度的变化

Fig. 10 Maximum stress of laser irradiated fused silica with scratch surface versus laser energy density

激光辐照平滑表面熔石英产生的应力。图11(a)给出了划痕深度d分别为1、2、3 μm时应力随划痕宽度的变化规律。随着划痕宽度的增大，熔石英内部应力变化的总体趋势为先增大后减小，在宽度为4 μm、深度为2 μm时应力达到最大。当划痕深度为2 μm和3 μm且宽度小于1 μm时，应力出现了异常的变化，即应力随划痕宽度的增大而减小。这是由于在划痕极端尖锐的情况下，熔石英内部应力聚集在划痕尖锐处，因此应力增大。图11(b)给出了划痕宽度w分别为2、4、6 μm时应力随划痕深度的变化规律。随着划痕深度的增大，熔石英内部应力先增大后减小，在深度为2 μm、宽度为4 μm时应力出现最大值。当划痕深度为0.05 μm时，激光辐照宽度为2、4、6 μm的表面划痕所产生的应力分别为9.1、9.4、9.3 MPa，与辐照平滑表面所产生的应力（虚线）8.7 MPa十分接近。从图11(a)、(b)可以看出，激光辐照划痕表面产生的应力会出现与划痕尺寸相关的增大。当划痕宽度为4 μm、深度为2 μm时应力达到最大值46.1 MPa，与激光辐照平滑表面产生的应力8.7 MPa相比增大了4倍。

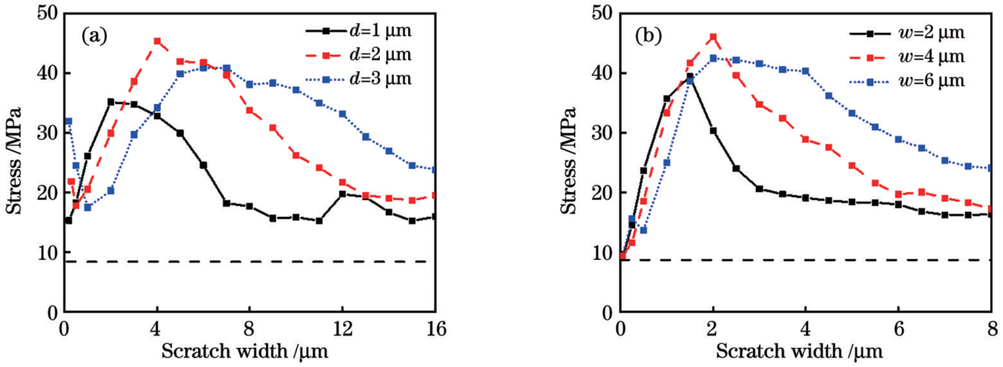

图11 划痕尺寸对激光辐照后熔石英应力的影响。(a)应力最大值随划痕宽度的变化；(b)应力最大值随划痕深度的变化

Fig. 11 Effects of scratch size on stress of fused silica after laser irradiation. (a) Maximum stress versus scratch width; (b) maximum stress versus scratch depth

4 结论

构建了激光辐照平滑表面和划痕表面光学材料的热应力模型，该模型可仿真计算纳秒激光与表面具有纳米、微米级划痕的熔石英之间的相互作用。利用所建模型研究了355 nm纳秒脉冲激光辐照平滑表面和划痕表面熔石英所产生的热应力特性，并且搭建激光损伤测试以及应力在线测量系统对该模型进行了验证。结果表明：所建的数值模型不仅可以准确地模拟激光辐照平滑表面熔石英所产生的应力分布，而且也可以模拟激光辐照划痕表面所产生的应力分布，且计算结果与实验测量结果一致。因此，利用该模型可以进一步仿真计算具有不同类型、不同尺寸缺陷或者各种周期性结构的光学材料与激光相互作用的热力学特性。另外，该模型计算结果还表明，表面划痕引起的光场调制导致激光辐照后温度升高和应力增大，温度场和应力场分布与其表面形貌密切相关。所构建的热应力模型及计算结果为激光加工的热应力调控提供了理论依据。

参考文献

[1] Mader M, Schlatter O, Heck B, et al. High-throughput injection molding of transparent fused silica glass[J]. Science, 2021, 372(6538): 182-186.

[2] Tan C, Zhao L J, Chen M J, et al. Physical mechanism of pulsed laser interaction with fused silica optics during CO$_2$ laser mitigation process[J]. Journal of Non-Crystalline Solids, 2021, 558: 120662.

[3] Song H W, Dan J Q, Li J L, et al. Experimental study on the cutting force during laser-assisted machining of fused silica based on the Taguchi method and response surface methodology[J]. Journal of Manufacturing Processes, 2019, 38: 9-20.

[4] 叶成, 邱荣, 蒋勇, 等. 1064 nm和532 nm纳秒激光同时辐照熔石英损伤规律的研究[J]. 强激光与粒子束, 2018, 30(4): 041003.
Ye C, Qiu R, Jiang Y, et al. Laser induced damage characteristics in fused silica surface irradiated by 1064 nm and 532 nm ns laser simultaneously[J]. High Power Laser and Particle Beams, 2018, 30(4): 041003.

[5] Negres R A, Norton M A, Cross D A, et al. Growth behavior of laser-induced damage on fused silica optics under UV, ns laser irradiation[J]. Optics Express, 2010, 18(19): 19966-19976.

[6] 曹珍, 贺洪波, 胡国行, 等. 多脉冲激光诱导熔石英体损伤的时

间分辨研究[J]. 中国激光, 2019, 46(8): 0803001.
Cao Z, He H B, Hu G H, et al. Time-resolved investigation of multiple-pulse laser-induced bulk damage in fused silica[J]. Chinese Journal of Lasers, 2019, 46(8): 0803001.

[7] 孙劭伟, 齐乃杰, 孔艳, 等. 熔石英玻璃激光损伤的三维应力场研究[J]. 中国激光, 2021, 48(1): 0101001.
Sun S W, Qi N J, Kong Y, et al. Three-dimensional stress fields of laser damaged fused silica[J]. Chinese Journal of Lasers, 2021, 48(1): 0101001.

[8] Zheng Y, Ma P, Li H B, et al. Studies on transmitted beam modulation effect from laser induced damage on fused silica optics [J]. Optics Express, 2013, 21(14): 16605-16614.

[9] Zhao L J, Cheng J, Chen M J, et al. Formation mechanism of a smooth, defect-free surface of fused silica optics using rapid CO_2 laser polishing[J]. International Journal of Extreme Manufacturing, 2019, 1(3): 035001.

[10] Veinhard M, Bonville O, Courchinoux R, et al. Quantification of laser-induced damage growth using fractal analysis[J]. Optics Letters, 2017, 42(24): 5078-5081.

[11] Lu Q, Lu F K, He X L, et al. Laser-pulse-induced temperature, thermal stress, and crater morphology effect during multipulse nanosecond laser manufacturing[J]. Applied Optics, 2022, 61(11): 2929-2936.

[12] Robin L, Combis P, Cormont P, et al. Infrared thermometry and interferential microscopy for analysis of crater formation at the surface of fused silica under CO_2 laser irradiation[J]. Journal of Applied Physics, 2012, 111(6): 063106.

[13] 陈明君, 王会尧, 程健, 等. 熔石英光学元件加工亚表面缺陷检测及抑制技术研究进展[J]. 机械工程学报, 2021, 57(20): 1-19.
Chen M J, Wang H Y, Cheng J, et al. Progress in detection and suppression techniques for processing-induced sub-surface defects of fused silica optical elements[J]. Journal of Mechanical Engineering, 2021, 57(20): 1-19.

[14] Chambonneau M, Rullier J L, Grua P, et al. Wavelength dependence of the mechanisms governing the formation of nanosecond laser-induced damage in fused silica[J]. Optics Express, 2018, 26(17): 21819-21830.

[15] Guignard F, Autric M L, Baudinaud V. Temperature and residual stress evolution in CO_2-laser-irradiated glass[J]. Proceedings of SPIE, 1998, 3343: 534-545.

[16] Gallais L, Cormont P, Rullier J L. Investigation of stress induced by CO_2 laser processing of fused silica optics for laser damage growth mitigation[J]. Optics Express, 2009, 17(26): 23488-23501.

[17] Zhu C Y, Liang L X, Yuan H, et al. Investigation of stress wave and damage morphology growth generated by laser-induced damage on rear surface of fused silica[J]. Optical Express, 2020, 28 (3): 3942-3951.

[18] Rehman Z U, Ullah S, Qayyum H, et al. Phase transformations initiated by optical breakdown in bulk of fused silica[J]. Optics & Laser Technology, 2021, 134: 106630.

[19] 吴朱洁, 潘云香, 赵竞元, 等. 毫秒激光辐射K9玻璃的激光损伤研究[J]. 红外与激光工程, 2019, 48(8): 0805005.
Wu Z J, Pan Y X, Zhao J Y, et al. Research on laser-induced damage of K9 glass irradiated by millisecond laser[J]. Infrared and Laser Engineering, 2019, 48(8): 0805005.

[20] Du Y, Wu X, Zhu M P, et al. Theoretical and experimental research on laser-induced damage of cylindrical subwavelength grating[J]. Optics Express, 2015, 23(19): 24296-24307.

[21] Li Z L, Xia Z L. The damage mechanism and process of metal multi-layer dielectric gratings induced by ps-pulsed laser[J]. Applied Surface Science, 2019, 494: 977-982.

[22] 叶鑫, 蒋晓东, 张继成, 等. 亚波长减反射光栅的研究进展[J]. 激光与光电子学进展, 2010, 47(6): 060501.
Ye X, Jiang X D, Zhang J C, et al. Research development of subwavelength antireflection gratings[J]. Laser & Optoelectronics Progress, 2010, 47(6): 060501.

[23] Bonod N, Brianceau P, Neauport J. Full-silica metamaterial wave plate for high-intensity UV lasers[J]. Optica, 2021, 8(11): 1372-1379.

[24] Ye X, Huang J, Geng F, et al. High power laser antireflection subwavelength grating on fused silica by colloidal lithography[J]. Journal of Physics D: Applied Physics, 2016, 49(26): 265104.

[25] Ye H, Li Y G, Xu Q, et al. Resistance of scratched fused silica surface to UV laser induced damage[J]. Scientific Reports, 2019, 9: 10741.

[26] Wang H X, Wang C, Zhang M Z, et al. Investigation of subsurface damage density and morphology impact on the laser-induced damage threshold of fused silica[J]. Applied Optics, 2019, 58(36): 9839-9845.

[27] Doualle T, Gallais L, Cormont P, et al. Thermo-mechanical simulations of CO_2 laser-fused silica interactions[J]. Journal of Applied Physics, 2016, 119(11): 113106.

[28] Zhang Y M, Shen Z H, Ni X W. Modeling and simulation on long pulse laser drilling processing[J]. International Journal of Heat and Mass Transfer, 2014, 73: 429-437.

[29] Rozenbaum O, Meneses D D S, Auger Y, et al. A spectroscopic method to measure the spectral emissivity of semi-transparent materials up to high temperature[J]. Review of Scientific Instruments, 1999, 70(10): 4020-4025.

[30] 冯小琴, 宋文爱, 马锦红. 光弹性技术测试应力[J]. 电子测试, 2009(2): 6-8, 14.
Feng X Q, Song W A, Ma J H. Photoelastic technology is used to measure stress[J]. Electronic Test, 2009(2): 6-8, 14.

[31] 齐乃杰, 袁晓东, 张丽娟, 等. 激光损伤残余应力三维检测技术[J]. 中国激光, 2020, 47(10): 1004001.
Qi N J, Yuan X D, Zhang L J, et al. Three-dimensional detection technology of laser damage residual stress[J]. Chinese Journal of Lasers, 2020, 47(10): 1004001.

Thermal Stress Model of Fused Silica with Scratch Surface Irradiated by Nanosecond Laser

Lu Qiang[1], Xu Weihong[2], Wang Shouyu[1], Kong Yan[1], Liu Cheng[1,3*]
[1]*Computational Optics Laboratory, School of Sciences, Jiangnan University, Wuxi* 214122, *Jiangsu, China*;
[2]*College of Internet of Things and Artificial Intelligence, Wuxi Vocational Institute of Commerce, Wuxi* 214153, *Jiangsu, China*;
[3]*Shanghai Institute of Optics and Fine Mechanics, Chinese Academy of Sciences, Shanghai* 201800, *China*

Abstract

Objective Lasers are widely used in laser processing, laser medical treatment, optical communication, inertial confinement, and nuclear fusion. With the continuous development of laser technology, the output power and single-pulse energy of lasers are increasing. Under high energy density conditions, the laser damage resistance of optical elements is one of the main factors affecting further development of high-power laser systems. Laser-induced damage shortens the working life of optical elements and considerably reduces the peak power output of high-power laser systems. Therefore, it is necessary to investigate the damage characteristics of optical materials under high-power laser irradiation. The mechanism of laser damage is very complicated and involves several physical processes, such as laser energy deposition, temperature and stress changes, and material phase transformation. During these processes, stress leads to damage of optical components, such as pits and cracks, and the residual stress in optical components increases the difficulty of laser repairing optical components. Therefore, it is crucial to investigate the thermal stress characteristics of laser-irradiated optical materials. However, current research on thermal stress properties is focused on optical materials with smooth surfaces, and the results are not applicable to uneven-surface optical elements with various defects and periodic structures. The thermal stress characteristics of complex surfaces under laser irradiation should be analyzed using thermodynamic models and related experiments.

Methods Based on the theories of electromagnetic fields, heat conduction, and elastic-plastic mechanics, thermal stress numerical models of optical materials are established for different types of nanosecond pulse laser irradiation to investigate the uneven-surface thermal stress characteristics of optical materials under laser irradiation. This thermal stress numerical model can simulate the temperature and stress field distributions of optical materials with smooth and uneven surfaces under laser irradiation. Moreover, it can analyze the modulation effect of the surface structure on the incident laser and the relationship between light field modulation and the temperature and stress fields. During laser irradiation, the energy absorbed by the material is regarded as a heat source. It considers the classical heat conduction and heat loss induced by heat convection and radiation to improve the accuracy of the model. Moreover, the thermal stress model reflects the diffraction and interference of the incident laser near the material surface structure by introducing the relative light intensity factor. The temperature and stress field distributions in optical materials can be determined by solving heat conduction and thermoelastic equations.

Results and Discussions The simulation results for fused silica with smooth surface irradiated by a single pulse indicate that when the laser energy distribution in the fused silica does not change, the temperature and stress distributions are consistent with the Gaussian distribution of laser energy (Fig. 2). The simulation results for fused silica with scratch surface under single-pulse irradiation show that owing to the light field modulation via surface scratching, the fused silica with scratch surface reaches the melting point at a low laser energy density, and the temperature and thermal stress fields in the scratch surface appear as streaking phenomena (Fig. 3). The simulation results for the stress induced by the smooth surface under laser irradiation are compared with the experimental results. The results demonstrate the accuracy of the proposed model for simulating the thermal stress characteristics of the fused silica with smooth surface induced by laser irradiation (Fig. 5). The experimental and simulation results for laser-irradiated fused silica with scratch surface also demonstrate the accuracy of the model for simulating the thermal stress characteristics of laser-irradiated scratch surfaces (Fig. 9). Under the same laser energy density irradiation, more significant stress is generated in the fused silica with scratch surface because of the modulation effect of the surface scratch on the incident laser, and the stress enhancement is related to the surface scratch size (Fig. 11).

Conclusions In this study, a thermal stress model is established to show the interaction between laser and optical materials with uneven surface. The thermal stress characteristics of the fused silica materials with a smooth surface and a scratch surface irradiated by a 355 nm nanosecond pulse laser are evaluated using the proposed model, and a laser damage test and stress online-measurement system are built to verify the model. The experimental and simulation results show that the established numerical model for the laser-material interaction can precisely simulate the stress distribution generated via laser irradiation on fused silica with smooth surface. The computed results for the stress distribution generated by laser irradiation on the scratch surface are consistent with the experimental results. Compared to that generated by the fused silica with smooth surface, the light field modulation generated by the fused silica with uneven surface enhances the thermal stress inside the fused silica after laser irradiation, and the size of the surface structure significantly influences the stress. The thermal stress model is valuable for analyzing the laser damage mechanism and residual stress of optical elements with uneven surfaces and provides a theoretical basis for controlling thermal stress during laser processing.

Key words laser technique; laser damage; stress distribution; surface scratch; light field modulation